Flux analysis of central metabolic pathways in the Fe (III)-reducing organism *Geobacter metallireducens* via ^{13}C isotopic labeling

†Yinjie J. Tang[1,2,7], †Romy Chakraborty[3,7], Héctor García Martín[4], Jeannie Chu[1,2], Terry C. Hazen[3,7], Jay D. Keasling[1,2,5,6,7,*]

[1]Synthetic Biology Department, Physical Biosciences Division, Lawrence Berkeley National Laboratory, Berkeley, CA 94720

[2]Department of Chemical Engineering, University of California at Berkeley, Berkeley, CA 94720

[3]Center for Environmental Biotechnology, Lawrence Berkeley National Laboratory, Berkeley, CA 94720

[4]DOE Joint Genome Institute, 2800 Mitchell Drive, Walnut Creek, CA 94598

[5]Department of Bioengineering, University of California at Berkeley, Berkeley, CA 94720

[6]California Institute for Quantitative Biomedical Research (QB3), University of California at Berkeley, Berkeley, CA 94720

[7] Virtual Institute for Microbial Stress and Survival, http://vimss.lbl.gov

[*]Corresponding author. Mailing address: Berkeley Center for Synthetic Biology, 717 Potter .Street, Building 977, Mail code 3224, University of California, Berkeley, CA 94720-3224. USA. Phone: (510) 495-2620. Fax: (510) 495-2630. E-mail: keasling@berkeley.edu.

† Equal contributions

Abstract

We analyzed the carbon fluxes in the central metabolism of *Geobacter metallireducens* strain GS-15 using ^{13}C isotopomer modeling. Acetate labeled in the 1st or 2nd position was the sole carbon source, and Fe-NTA was the sole terminal electron acceptor. The measured labeled acetate uptake rate was 21 mmol/gdw/h in the exponential growth phase. The resulting isotope labeling pattern of amino acids allowed an accurate determination of the *in vivo* global metabolic reaction rates (fluxes) through the central metabolic pathways using a computational isotopomer model. The model indicated that over 90% of the acetate was completely oxidized to CO_2 via a complete tricarboxylic acid (TCA) cycle while reducing iron. Pyruvate carboxylase and phospho*enol*pyruvate carboxykinase were present under these conditions, but enzymes in the glyoxylate shunt and malic enzyme were absent. Gluconeogenesis and the pentose phosphate pathway were mainly employed for biosynthesis and accounted for less than 3% of total carbon consumption. The model also indicated surprisingly high reversibility in the reaction between oxoglutarate and succinate. This step operates close to the thermodynamic equilibrium possibly because succinate is synthesized via a transferase reaction, and its product, acetyl-CoA, inhibits the conversion of oxoglutarate to succinate. These findings enable a better understanding of the relationship between genome annotation and extant metabolic pathways in *G. metallireducens.*

Key words: labeled acetate, electron acceptor, minimal medium, TCA cycle, acetyl-CoA transferase

Introduction

Geobacter species have been known to be one of the dominant groups of microorganisms mediating iron reduction in the environment (20). They have been found to be ubiquitous in a myriad of subsurface environments. Detailed studies of their metabolism has revealed them to be capable of bioremediation of several heavy metals including uranium, plutonium, technitium, and vanadium as well as biodegradation of several organic contaminants including monoaromatic hydrocarbons (15, 16, 25). More recently, *Geobacter* species have been used to generate electricity from waste organic matter (2, 14, 18). These unique metabolisms make *Geobacter* species important players in the contaminated subsurface environment (17). *Geobacter metallireducens* was the first iron-reducing organism isolated that coupled oxidation of organic acids to reduction of iron oxides (19, 20). It completely oxidizes organic carbons such as fatty acids, alcohols and monoaromatic compounds via the tricarboxylic acid (TCA) cycle (3, 19) coupled with the reduction of iron. The genomes of several *Geobacter* species have been sequenced, and proteome data are also available (5, 23). While the genome sequence and proteome are important for understanding *Geobacter*, they are not necessarily accurate representations of cell physiology and metabolism.

To quantitatively analyze central metabolism in *Geobacter sulfurreducens,* a constraint-based model was developed using the annotated genome sequence and a series of physicochemical constraints (thermodynamic directionality, enzymatic capacity and reaction stoichiometry) (21). While the model provided important insight into energy conservation, biosynthesis of building blocks (such as amino acids), and the relationship of the genotype to its phenotype, underdetermined models require one to assume an objective function (i.e., maximizing the specific growth rate) that may or may not be accurate and have difficulty

predicting fluxes through reversible reactions or reactions that may form futile cycles (7, 31, 38). Further, genes are often incorrectly annotated in sequenced genomes, and incorporation of these reactions into the model can affect the flux calculation. Even when properly annotated, the presence of a gene does not indicate if it is being expressed.

Here we report a different approach to analyze the fluxes in the central metabolic pathways of *Geobacter metallireducens* GS-15. The cells were fed [^{13}C]acetate, and the distribution of the ^{13}C was measured in amino acids. Interpreted in the light of the genome annotation, a model based on the atom transitions between metabolites in biochemical reactions calculated the fluxes through the central metabolic pathway (11, 31, 32, 34). The model did not require energy balances for the calculation and resolved bidirectional or futile reactions. This study provided complementary flux information to the recent *in silico* model predictions, and further extended our understanding of anaerobic carbon metabolism in *Geobacter* species.

Materials and methods

Growth conditions. All media and solutions were prepared using strict anaerobic techniques. The standard *Geobacter metallireducens* bicarbonate-buffered freshwater medium was used (20) with one exception: one-tenth of the vitamin mix solution was used. Briefly, the medium was boiled under a N_2-CO_2 (80-20, vol/vol) headspace in order to remove the dissolved oxygen. It was then dispensed into anaerobic pressure tubes or serum bottles under a N_2-CO_2 (80-20, vol/vol) headspace. The anaerobic pressure tubes or serum bottles were capped with thick butyl-rubber stoppers and sterilized. [1-^{13}C] Sodium acetate and [2-^{13}C] sodium acetate (both of 99% purity) were obtained from Cambridge Isotope Laboratories Inc. Anoxic aqueous stock solutions were prepared of Ferric-NTA (1M), [1-^{13}C] or [2-^{13}C] sodium acetate (1 M)

under a headspace of N_2-CO_2. These stocks were delivered anaerobically into culture tubes and serum bottles via a needle. *G. metallireducens* GS-15 was routinely cultured on anaerobic basal medium (20) using 5 mM acetate and 15 mM Fe-NTA as the electron donor and acceptor, respectively, under a N_2-CO_2 (80:20, vol:vol) headspace. A 10% inoculum from the unlabeled stock culture was made into the [1-^{13}C] or [2-^{13}C] acetate medium containing equivalent amounts of electron donor and acceptor. After growth reached the mid-log phase, cells were transferred again into the same labeled medium to minimize the effect of unlabeled carbon from the initial inoculum. This sub-culture protocol was repeated twice. All incubations were performed at 30°C.

Determining metabolite concentrations and biomass composition. The standard ferrozine assay was used to measure Fe(II) concentration during growth on acetate and Fe-NTA (20). Cell counts were performed using a microscope and acridine orange to stain cells. Briefly, a 100-µl sample was added to 900 µl 0.1% sodium polyphosphate solution and mixed well. 10 µl of this cell suspension was pipetted onto a 6 mm well of slide. The slide was dried and heat fixed. Twenty-five (25) µl of acridine orange stain was used to stain the wells containing several dilutions of the cell samples. The slides were incubated in the dark for 2 minutes, washed, and then dried; the cells were counted using fluorescent microscopy. The concentrations of acetate in the culture supernatant (following centrifugation of the culture at 10,000 × g for 20 minutes at 4°C) were measured using enzyme assays (r-Biopharm, Darmstadt, German). The amino acid composition of the biomass protein was quantified using the Beckman 6300 amino acid analyzer (Beckman Coulter, California), performed by the Molecular Structure Facility at the University of California, Davis. Biomass constituents were taken from the literature: protein (46%), RNA

(10%), DNA (4%), lipids (15%), total carbohydrate (15%), lipopolysaccharides (4%), and peptidoglycan (4%) (21).

Isotopomer analysis of protein amino acids by GC-MS (32-34)**.** A 200-mL cell culture (cell number 2×10^8) was harvested by centrifugation at 10,000 × g for 20 minutes at 4°C and sonicated subsequently for 3 minutes. The protein from the resulting lysate was precipitated using trichloroacetic acid and then hydrolyzed in 6 M HCl at 100°C for 24 hours. The amino acid/HCl solution was dried under nitrogen flow overnight. GC-MS samples were prepared in 100 µl of tetrahydrofuran (THF) and 100 µl of N-(tert-butyldimethylsilyl)-N-methyl-trifluoroacetamide (Sigma-Aldrich, USA). These samples were derivatized at 70°C for 1 hour, producing tert-butyldimethlysilyl (TBDMS) derivatives (32-34). One µL of the derivatized sample was injected into the gas chromatograph (Agilent, model HP6890) equipped with a DB5-MS column (J&W Scientific, Falsom CA) and analyzed using a mass spectrometer (Agilent, model 5973). The GC column was held at 150°C for 2 minutes, heated at 3°C per minute to 280°C, heated at 20°C per minute to 300°C, and held for 5 minutes at that temperature.

Annotated pathway map and algorithm for flux calculation. The key biochemical pathways in *Geobacter metallireducens* GS-15 include gluconeogenesis, the TCA cycle, and the pentose phosphate (PP) pathway (1). Each reaction and its corresponding gene are listed in Supplementary Table S-1. The fluxes through the pool of amino acids, carbohydrate, and RNA/DNA were loosely constrained by the biomass production and the measured average biomass composition (Supplementary Table S-2). The reversible reactions were characterized by their net flux, v_i, and their exchange flux, v_i^{exch}. The net flux is defined as the difference between forward and backward fluxes, ($v_i^{\rightarrow}$- $v_i^{\leftarrow}$). The exchange flux, v_i^{exch}, is the smaller of the forward

and backward fluxes, min($v_i^{\rightarrow}$, $v_i^{\leftarrow}$) and is used to calculate the exchange coefficient, $exch_i$, according to (32, 37)

$$v_i^{exch} = \frac{exch_i}{1 - exch_i} \quad (1)$$

Exchange coefficients for some key reactions were searched globally in the range [0 1] (40). The steady-state isotopomer distributions in the intracellular metabolite pools for a given flux distribution were obtained via the isotopomer mapping matrices (28) (using MATLAB 6.0, Mathworks, USA); these isotopomer distributions were used to simulate MS data (m/z=M0, M1, M2…). The optimal solution was found based on an objective function defined as:

$$\varepsilon(v_n) = \sum_{i=1}^{a} \left(\frac{M_i - N_i(v_n)}{\delta_i} \right)^2 \quad (2)$$

where v_n are the unknown fluxes to be optimized in the program, M_i are the measured MS data when [1-^{13}C] or [2-^{13}C]acetate was used as the carbon source, respectively; N_i are the corresponding model-simulated MS data; and δ_i are the corresponding measurement errors. The flux estimations were calculated to be such that ε was minimized using a simulated annealing approach with different initial conditions (26, 32). The initial annealing temperature was set to 50 and the final one to 0.01, with the temperature being decreased 100 times by a set fraction each time. In each run, 10,000~100,000 moves were used, and the algorithm was restarted from the final position several times to check the reliability of the minimum. The MATLAB programs for calculation of flux and exchange coefficients are available at http://vimss.lbl.gov/DvHFlux/AdvancedCodesWithAMM_IMM.rar. The solution produced isotopomer predictions consistent with measured data from both [1-^{13}C] and [2-^{13}C] acetate experiments.

Result and discussion

***Geobacter metallireducens* GS-15 growth kinetics in minimal medium.** GS-15 grew in minimal medium and completely oxidized acetate as the sole carbon and energy source by reducing Fe^{3+} to Fe^{2+} (Figure 1). The doubling time was ~5 hours with a late mid-log phase density of ~2.3×10^8 cells/ml, and the corresponding biomass concentration was 4.8±0.3 mg/L with yield of 3.2 gdw/mol acetate. In the final sampling point, about 1.5 mM acetate was consumed and 11 mM Fe^{2+} was generated (equivalent to dissimilating 1.4 mM acetate). This result indicates that the Geobacter's biomass yield from oxidization of acetate is three times lower than the thermodynamic yield predictions (16.8 gdw/mol acetate) (35, 39). Although Fe^{3+} (ΔG^{Θ}=-24.38 kcal/eq) has a similar electron potential as oxygen (ΔG^{Θ}=-25.28 kcal/eq) (22), the electrons are transported outside of the cell or into the periplasmic cytochrome pool, but the protons remains in the cytoplasm (21). This could result in acidification of the cytoplasm, which in turn could reduce the membrane potential and the biomass that results from acetate via Fe^{3+} reduction compared to that obtained during oxygen or fumarate reduction conditions (8, 21).

***Isotopomer analysis of labeling pattern in protein amino acids by GC-MS*.** Labeled acetate (1^{st} position or 2^{nd} position) was used in independent experiments. GS-15 was harvested in the exponential growth phase from each batch culture (a quasi steady state) (9, 27, 30). Two types of positively charged amino acid species from the biomass protein were clearly observed by GC-MS: unfragmented amino acids [M-57] and fragmented species [M-159] that had lost the α-carboxyl group (4, 6, 13, 36). The natural abundance of heavy isotopes common in organic molecules as well as the derivatization agents was corrected for by using published algorithms (36). The corrected GC-MS data for eight key amino acids useful for model calculation including $[M-57]^+$ and $[M-159]^+$ are provided (Table 1). The isotopomer distributions in the

amino acids from hydrolyzed protein were used to examine the metabolic pathways. For example, the different labeling patterns of alanine and serine indicate that their precursors were not same; i.e., alanine is derived from pyruvate, while serine is derived from PGA. In each type of experiment, isotopomer patterns in some amino acids from the same precursor were similar and provided redundant isotopomer information (10): i.e., threonine and aspartate from oxaloacetate, tyrosine and phenylalanine from phosphoenolpyruvate and erythrose-4-phosphate. Therefore, only one from each precursor listed in the table was used for model calculations. GC-MS cannot measure the ion fragment (M-57)+ (no loss, m/z=302) for leucine and isoleucine, accurately because of the overlay of mass peaks (mass fragment with only α and β carbon of leucine/isoleucine also has m/z=302) (36).

Determination of the flux distribution using the isotopomer model. The published annotated genome sequence of *Geobacter metallireducens* indicates that several amino acid biosynthesis pathways (e.g., lysine, valine, leucine, isoleucine and alanine) are incomplete (1). However, *Geobacter metallireducens* is able to grow in minimal medium with acetate as its sole carbon source, and therefore must contain complete energy and biosynthesis pathways for essential metabolism. The model calculation from two tracer experiments (with [1-^{13}C]acetate and [2-^{13}C]acetate) gave similar flux distribution results (Figure 2). The predicted labeling patterns of all metabolites, based on calculated fluxes and exchange coefficients, matched relatively well the measured data (deviations are within the noise from triplicate tracer experiments), and this indicates that model calculations are of good quality (Figure 3).

The conversion of acetate to acetyl-CoA (acetate uptake rate of 21±1.6 mmol/gdw/h, assumed to be 100 in the model calculation) may be catalyzed by two independent enzymes (acetyl-CoA transferase or acetate kinase) (Figure 2). The acetyl-CoA produced branched into

three pathways. The major flow (19 mmol/gdw/h, v= ~90) was into a complete TCA cycle; the second flow is (1.7 mmol/gdw/h, v= ~8) to pyruvate via pyruvate-ferredoxin oxidoreductase; and the third flow towards biomass production (e.g., synthesis of leucine and fatty acids). The genome annotation indicated that some key enzymes in gluconeogenesis were missing (EC 4.1.2.13 fructose-bisphosphate aldolase, EC2.7.2.3 phosphoglycerate kinase, EC5.4.2.4 bisphosphoglycerate synthase; i.e., no reactions for glycerate-3P → glycerate-1,3-P_2 and glyceraldehyde-3P → β-D-fructose-1,6-P_2). However, the tracer experiments indicated that gluconeogenesis is actually complete, and the total flux was 0.5 mmol/gdw/h (v=~2.5). The pentose phosphate pathway (PPP) is mainly used for biosynthesis when acetate is used as the single carbon source. Although there are several alternative pathways to make C5P (precursors of histidine and nucleotides), the model indicates that the major carbon flow to PPP is via the oxidative branch G6P→6PG→C5P, which generates NADPH. In general, the isotopomer model gave results consistent with the previous predictions from a constraints-based model for a closely related species, *Geobacter sulfurreducens* (21). However, the presence of phospho*enol*pyruvate carboxykinase was not predicted by the constraints-based model, but was determined using the isotopomer model.

Characterization of GS-15 metabolism under Fe^{3+} reduction conditions. Previous reports indicate that Geobacter posses two acetyl-CoA formation routes (via acetyl-CoA transferase or acetate kinase/P-transacetylase) to secure sufficient flux for growth, whereas other acetate-degrading anaerobic bacteria often use one pathway for acetyl-CoA formation. This study also indicates the flexibility of central metabolism in other carbon utilization routes. For example, pyruvate carboxylase activity was present (0.7 mmol/gdw/h, v=~3.6) — this is an alternative pathway to feed carbon into the TCA cycle by consuming ATP. Second, two carbon

flows lead to phospho*enol*pyruvate synthesis via pyruvate kinase / phospho*enol*pyruvate synthase (~0.4 mmol/gdw/h, v=~1.8) or phospho*enol*pyruvate carboxykinase (~0.1 mmol/gdw/h, v=~0.6). The presence of redundant pathways may stabilize cellular metabolism under conditions of environmental uncertainty (32). Meanwhile, the absence of the glyoxylate shunt (this pathway is not annotated) was confirmed by the isotopomer analysis. On the other hand, the $NADP^+$-dependent malic enzyme, which is inhibited by the presence of acetyl-CoA (12) and whose corresponding gene was annotated in the genome, had no flux. These results are consistent with the predictions from the genome-scale, constraints-based model (21). With respect to energy production, zero flux through the glyoxylate shunt and malic enzyme maximizes the total carbon flow through the oxidative TCA cycle and thus produces the most energy (NADH).

In general, decarboxylation reactions, such as the oxidative pathways in pentose phosphate and the TCA cycle, are frequently irreversible (29). However, the model predicted extremely high reversibility (exch=0.99) in the reaction from oxoglutarate to succinate compared to that in other microorganisms (40). This reaction contains two steps and is usually catalyzed by the enzymes oxoglutarate oxidoreductase (oxoglutarate → succinyl-CoA, ΔG^{Θ}=-33.5kJ/mol) and succinyl-CoA synthetase (succinyl-CoA→ succinate, ΔG^{Θ}= -2.9 kJ/mol) (24). The free energy of both steps indicates a positive driving force for converting oxoglutarate to succinate. However, the succinyl-CoA synthetase activity is absent in *Geobacter metallireducens*, and acetyl-CoA transferase instead is used to complete the reaction: succinyl-CoA (+acetate) → succinate (+acetyl-CoA) (12). The reason for the very high reversibility between oxoglutarate and succinate is likely that the accumulation of acetyl-CoA forces the reaction in the reverse direction, and thus inhibits the rate of carbon metabolism through TCA cycle. This may explain

the slow growth of *Geobacter metallireducens* under iron-reducing conditions, even though the organism can use the complete TCA cycle to oxidize carbon substrates similar to other aerobic bacteria.

Growth of *G. metallireducens* while oxidizing acetate requires incorporation of the CO_2 produced into biomass (acetyl-CoA + CO_2 → pyruvate and pyruvate + CO_2 → oxaloacetate), and our model also evaluated the fate of the labeled ^{13}C of carbon dioxide. Both experiments with [1-^{13}C] and [2-^{13}C] acetate showed that the [^{13}C]CO_2 in the medium was below 3% of total CO_2 (Table 1). This is consistent with the fact that the labeled $^{13}CO_2$ produced from acetate oxidization is negligible compared to the $^{12}CO_2$ from the headspace gases (N_2-CO_2). The experiment performed with [1-^{13}C]acetate introduced very little ^{13}C (<3%) into the C1 pool (5,10-Me-THF), while most of the C1 pool was labeled (82%) in the [2-^{13}C]acetate experiments. This result confirms that C1 metabolism is mainly via the serine pathway, i.e., serine is converted to glycine and a C1-unit before being incorporated into protein. The carbon transition routes are $^{*}CH_3COOH$ → $^{*}CH_3COCOOH$ → $^{*}CH_2(OH)CH(NH_2)COOH$ → CH_2NH_2COOH + *C1 pool.

In conclusion, this study demonstrates ^{13}C metabolic flux analysis as a tool for verifying genome annotation, characterizing the physiological state of microorganisms, and mapping the central metabolism in anaerobic bacteria. The results from our technique provide valuable complementary information to previous genome-based modeling approaches resulting in a comprehensive understanding of central carbon metabolism in microorganisms.

Acknowledgements

We thank Dr. M. Coppi in Dr. Derek Lovley group (Department of Microbiology, University of Massachusetts, Amherst) for advice on *Geobacter* anaerobic pathways. We also thank Michelle

Chang and Ding Chen (Department of Chemical Engineering, University of California, Berkeley) for helping with some experiments. This work is part of the Virtual Institute for Microbial Stress and Survival (http://VIMSS.lbl.gov) supported by the U.S. Department of Energy, Office of Science, Office of Biological and Environmental Research, Genomics: GTL Program through contract DE-AC02-05CH11231 between the Lawrence Berkeley National Laboratory and the US Department of Energy.

References

1. **Alm, E. J., K. H. Huang, M. N. Price, R. P. Koche, K. Keller, I. L. Dubchak, and A. P. Arkin.** 2005. The MicrobesOnline Web site for comparative genomics. Genome Res. **15:**1015-1022.
2. **Bond, D. R., D. E. Holmes, L. M. Tender, and D. R. Lovley.** 2002. Electrode-reducing microorganisms that harvest energy from marine sediments. Science **295:**483-485.
3. **Childers, S. E., S. Ciufo, and D. R. Lovley.** 2002. *Geobacter metallireducens* access insoluble Fe(III) oxide by chemotaxis. Nature **416:**767-769.
4. **Daunder, M., and U. Sauer.** 2000. GC-MS analysis of amino acids rapidly provides rich information for isotopomer balancing. Biotechnology Progress **16:**642-649.
5. **Ding, Y. H., K. K. Hixson, C. S. Giometti, S. A., A. Esteve-Nunez, T. Khare, S. L. Tollaksen, W. Zhu, J. N. Adkins, M. S. Lipton, R. D. Smith, T. Mester, and D. R. Lovley.** 2006. The proteome of dissimilatory metal-reducing microorganism *Geobacter sulfurreducens* under various growth conditions. Biochim Biophys Acta **1764:**1198-206.
6. **Dookeran, N. N., T. Yalcin, and A. G. Harrison.** 1996. Fragmentation reactions of protonated α-amino acids. Journal of Mass Spectrometry **31:**500-508.
7. **Edwards, J. S., and B. O. Palsson.** 2000. The *Escherichia coli* MG1655 *in silico* metabolic genotype: Its definition, characteristics, and capabilities. PNAS **97:**5528–5533.
8. **Esteve-Nunez, A., M. Rothermich, M. Sharma, and D. R. Lovley.** 2005. Growth of *Geobacter sulfurreducens* under nutrient-limiting conditions in continuous culture. Environ Microbiol. **7:**641-8.
9. **Fischer, E., and U. Sauer.** 2005. Large-scale *in vivo* flux analysis shows rigidity and suboptimal performance of *Bacillus subtilis* metabolism. Nature Genetics **37:**636-640.
10. **Fischer, E., and U. Sauer.** 2003. Metabolic flux profiling of *Escherichia coli* mutants in central carbon metabolism using GC-MS. Euro. J. Biochem **270:**880-891.
11. **Fuhrer, T., E. Fischer, and U. Sauer.** 2005. Experimental identification and quantification of glucose metabolism in seven bacterial species. Journal of Bacteriology **187:**1581-1590.

12. **Galushko, A. S., and B. Schink.** 2000. Oxidation of acetate through reactions of the citric acid cycle by *Geobacter sulfurreducens* in pure culture and in syntrophic coculture. Arch. Microbiol. **174:**314-321.
13. **Harrison, A. G.** 2001. Ion chemistry of protonated glutamic acid derivatives. International Journal of Mass Spectrometry **210/211:**361-370.
14. **Holmes, D. E., D. R. Bond, R. A. O'Neil, C. E. Reimers, L. R. Tender, and D. R. Lovley.** 2004. Microbial communities associated with electrodes harvesting electricity from a variety of aquatic sediments. Microbial Ecology **48:**178-190.
15. **Lloyd, J. R., J. Chesnes, S. Glasauer, D. J. Bunker, F. R. Livens, and D. R. Lovley.** 2002. Reduction of Actinides and Fission Products by Fe(III)-Reducing Bacteria. Geomicrobiology Journal **19:**103-120.
16. **Lloyd, J. R., V. A. Sole, C. V. G. Van Praagh, and D. R. Lovley.** 2000. Direct and Fe(II)-Mediated Reduction of Technetium by Fe(III)-Reducing Bacteria. Applied and Environmental Microbiology **66:**3734-3749.
17. **Lovley, D. R.** 2003. Cleaning up with genomics: applying molecular biology to bioremediation. Nat. Rev. Microbiol. **1:**35-44.
18. **Lovley, D. R., and R. T. Anderson.** 2000. Influence of dissimilatory metal reduction on the fate of organic and metal contaminants in the subsurface. Hydogeol. J. **8:**77-88.
19. **Lovley, D. R., S. J. Giovannoni, D. C. White, J. E. Champine, E. J. Phillips, Y. A. Gorby, and S. Goodwin.** 1993. *Geobacter metallireducens* gen. nov. sp. nov., a microorganism capable of coupling the complete oxidation of organic compounds to the reduction of iron and other metals. Arch. Microbiol. **159:**336-344.
20. **Lovley, D. R., and E. J. P. Phillips.** 1988. Novel mode of microbial energy metabolism: organic carbon oxidation coupled to dissimilatory reduction of iron or manganese. Applied and Environmental Microbiology **54:**1472-1480.
21. **Mahadevan, R., D. R. Bond, J. E. Butler, A. Esteve-Nunez, M. V. Coppi, B. O. Palsson, C. H. Schilling, and D. R. Lovley.** 2006. Characterization of metabolism in the Fe(III)-reducing organism *Geobacter sulfurreducens* by constraint-based modeling. Applied and Environmental Microbiology **72:**1558-68.
22. **McFarland, M. J., and R. C. Sims.** 1991. Thermodynamic Framework for Evaluating PAH Degradation in the Subsurface. Ground Water **29:**885-896.
23. **Methe, B. A., K. E. Nelson, J. A. Eisen, I. T. Paulsen, W. Nelson, J. F. Heidelberg, D. Wu, M. Wu, N. Ward, M. J. Beanan, R. J. Dodson, R. Madupu, L. M. Brinkac, S. C. Daugherty, R. T. DeBoy, A. S. Durkin, M. Gwinn, J. F. Kolonay, S. A. Sullivan, D. H. Haft, J. Selengut, T. M. Davidsen, N. Zafar, O. White, B. Tran, C. Romero, H. A. Forberger, J. Weidman, H. Khouri, T. V. Feldblyum, T. R. Utterback, S. E. Van Aken, D. R. Lovley, and C. M. Fraser.** 2003. Genome of *Geobacter sulfurreducens*: metal reduction in subsurface environments. Science **302:**1967-9.
24. **Nelson, D. L., and M. M. Cox.** 2000. Lehninger Principles of Biochemistry. Worth Publishers, New York.
25. **Ortiz-Bernad, I., R. T. Anderson, H. Vrionis, and D. R. Lovley.** 2004. Vanadium Respiration by *Geobacter metallireducens*: Novel Strategy for *In Situ* Removal of Vanadium from Groundwater. Applied and Environmental Microbiology **70:**3091-3095.
26. **Press, W. H., S. A. Teukolsky, W. T. Vetterling, and B. P. Flannery.** 1992. Numerical Recipes in FORTRAN, 2nd ed. Cambridge University Press, Cambridge.

27. **Sauer, U., D. R. Lasko, J. Fiaux, M. Hochuli, R. Glaser, T. Szyperski, K. Wuthrich, and J. E. Bailey.** 1999. Metabolic flux ratio analysis of genetic and environmental modulations of Escherichia coli central carbon metabolism. Journal of Bacteriology **181:**6679-6688.
28. **Schmidt, K., M. Carlsen, J. Nielsen, and J. Villadsen.** 1997. Modeling isotopomer distributions in biochemical networks using isotopomer mapping matrices. Biotechnology and Bioengineering **55:**831-840.
29. **Schmidt, K., J. Nielsen, and J. Villadsen.** 1999. Quantitative analysis of metabolic fluxes in *Escherichia coli*, using two-dimensional NMR spectroscopy and complete isotopomer models. Journal of Biotechnology **71:**175-190.
30. **Stelling, J., U. Sauer, Z. Szallasi, F. Doyle, and J. Doyle.** 2004. Robustness of cellular functions. Cell **118:**675-685.
31. **Stephanopoulos, G. N., A. A. Aristidou, and J. Nielsen.** 1998. Metabolic Engineering Principles and Methodologies. Academic Press, San Diego.
32. **Tang, Y. J., J. S. Hwang, D. Wemmer, and J. D. Keasling.** 2006. The *Shewanella oneidensis* MR-1 fluxome under various oxygen conditions. Applied and Environmental Microbiology **In Press**.
33. **Tang, Y. J., A. L. Meadows, J. Kirby, and J. D. Keasling.** 2007. Anaerobic central metabolic pathways in *Shewanella oneidensis* MR-1 reinterpreted in the light of isotopic metabolite labeling. Journal of Bacteriology **In Press**.
34. **Tang, Y. J., F. Pingitore, A. Mukhopadhyay, R. Phan, T. C. Hazen, and J. D. Keasling.** 2007. Pathway confirmation and flux analysis of central metabolic pathways in *Desulfovibrio vulgaris* Hildenborough using GC-MS and FT-ICR mass spectrometry. Journal of Bacteriology **In press**.
35. **VanBriesen, J. M.** 2002. Evaluation of methods to predict bacterial yield using thermodynamics. Biodegradation **13:**171-190.
36. **Wahl, S. A., M. Dauner, and W. Wiechert.** 2004. New tools for mass isotopomer data evaluation in ^{13}C flux analysis: mass isotope correction, data consistency checking, and precursor relationships. Biotechnology and Bioengineering **85:**259-68.
37. **Wiechert, W., and A. A. de Graaf.** 1997. Bidirectional reaction steps in metabolic networks I. Modeling and simulation of carbon isotope labeling experiments. Biotechnology and Bioengineering **55:**101-117.
38. **Wiechert, W., M. Mollney, S. Petersen, and A. A. de Graaf.** 2001. A Universal Framework for ^{13}C Metabolic Flux Analysis. Metabolic Engineering **3:**265-283.
39. **Xiao, J., and J. M. VanBriesen.** 2005. Expanded thermodynamic model for microbial true yield prediction. Biotechnology and Bioengineering **93:**110-121.
40. **Zhao, J., and K. Shimizu.** 2003. Metabolic flux analysis of *Escherichia coli* K12 grown on 13C-labeled acetate and glucose using GC-MS and powerful flux calculation method. Journal of Biotechnology **101:**101-117.

Figure Captions

Figure 1. *Geobacter metallireducens* GS-15 growth kinetics in minimal medium: □, total cell number; ♦, Fe^{2+} concentration; ▲, acetate concentration.

Figure 2. Metabolic flux distribution in *Geobacter metallireducens* GS-15 under Fe^{3+} reduction conditions. The upper number indicates flux based on [1-^{13}C] acetate experiments, and the lower number indicates flux based on [2-^{13}C] acetate experiments. The acetate uptake rate was 21 mmol/gdw/h. The data in brackets are the exchange coefficients. The dotted arrows indicate the absence of an annotated gene for the step. Abbreviations: 6PG, 6-phosphogluconate; ACoA, acetyl-coenzyme A; C1, 5,10-Me-THF; C5P, ribose-5-phosphate (or ribulose-5-phosphate or xylulose-5-phosphate); CIT, citrate; E4P, erythrose-4-phosphate; F6P, fructose-6-phosphate; G6P, glucose-6-phosphate; ICT, isocitrate; MAL, malate; OAA, oxaloacetate; OXO, 2-oxoglutarate; PEP, phosphoenolpyruvate; PGA, 3-phosphoglycerate; PYR, pyruvate. S7P, sedoheptulose-7-phosphate; SUC, succinate; T3P, triose-3-phosphate.

Figure 3. Model quality test. ♦, glutamate data; □, aspartic acid data; ◊, alanine and leucine data; Δ, serine and glycine data; ×, histidine data; ○, phenyalanine data. The absolute GC-MS measurement errors were based on the information in Table 1.

Figure 1.

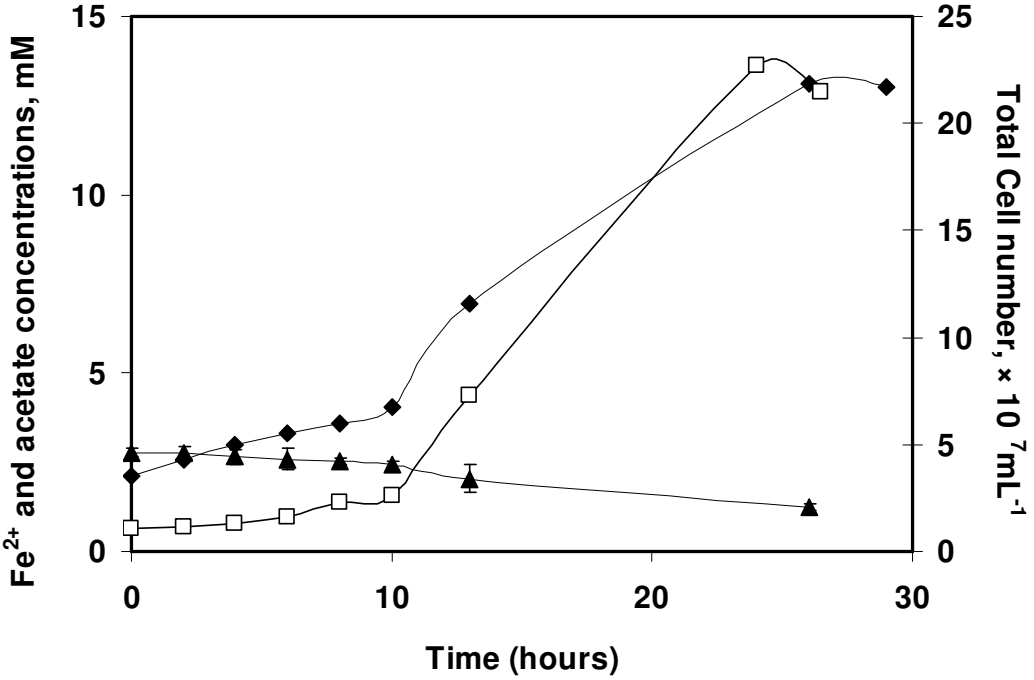
15
10
5
0
25
20
15
10
5
0
0
10
20
30
Time (hours)
Fe2+ and acetate concentrations, mM
Total Cell number, × 10 7mL-1

Figure 2.

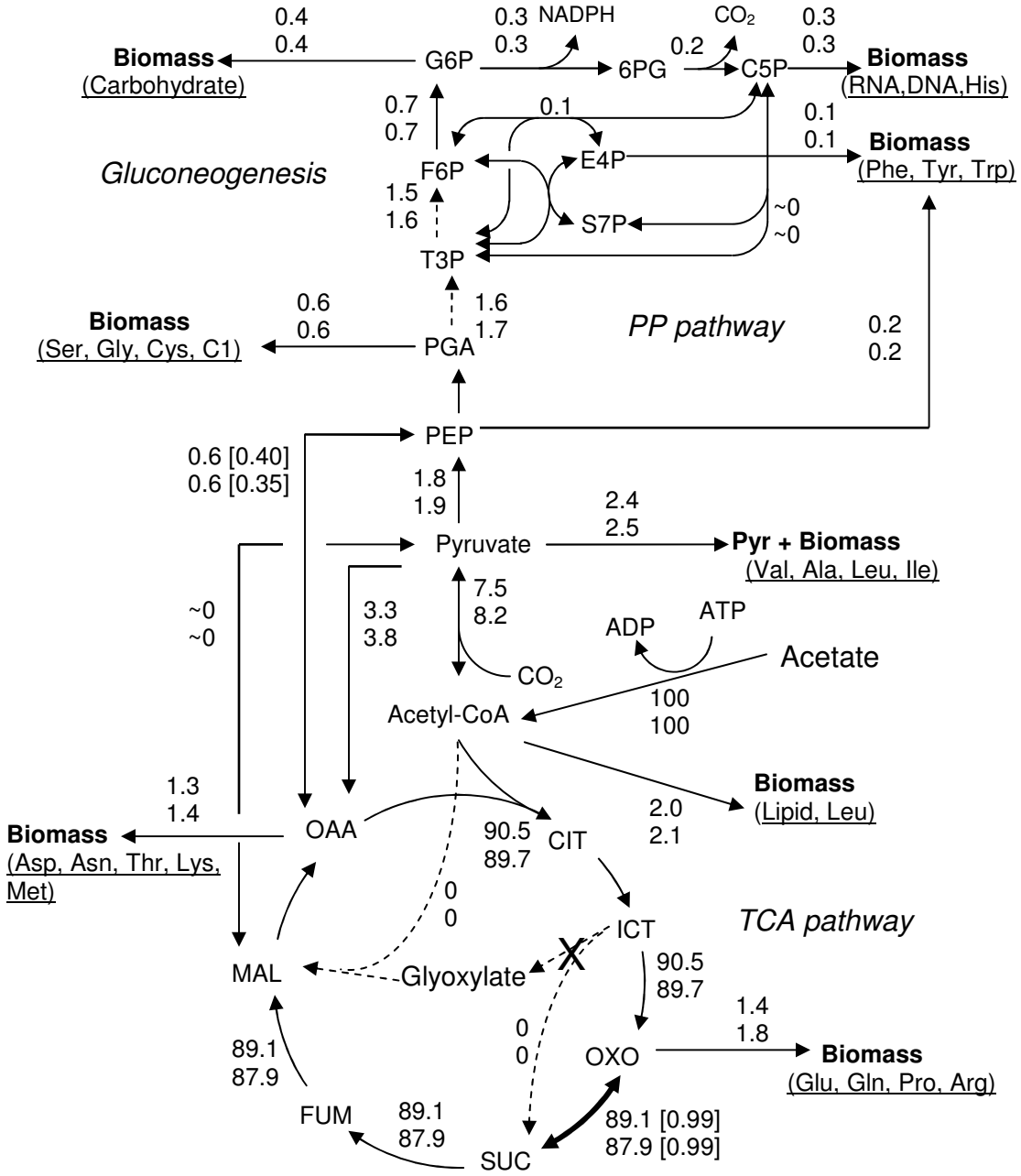
0.4
0.4
Biomass
(Carbohydrate)
G6P
0.3 NADPH
0.3
6PG
CO2
0.2
C5P
0.3
0.3
Biomass
(RNA,DNA,His)
0.7
0.7
0.1
0.1
0.1
Biomass
(Phe, Tyr, Trp)
Gluconeogenesis
F6P
E4P
1.5
1.6
S7P
~0
~0
T3P
Biomass
(Ser, Gly, Cys, C1)
0.6
0.6
PGA
1.6
1.7
PP pathway
0.2
0.2
PEP
0.6 [0.40]
0.6 [0.35]
1.8
1.9
2.4
2.5
Pyruvate
Pyr + Biomass
(Val, Ala, Leu, Ile)
~0
~0
3.3
3.8
7.5
8.2
ADP
ATP
Acetate
CO2
100
100
Acetyl-CoA
1.3
1.4
Biomass
(Lipid, Leu)
2.0
2.1
Biomass
(Asp, Asn, Thr, Lys,
Met)
OAA
90.5
89.7
CIT
0
0
ICT
TCA pathway
MAL
Glyoxylate
90.5
89.7
1.4
1.8
0
0
89.1
87.9
OXO
Biomass
(Glu, Gln, Pro, Arg)
FUM
89.1
87.9
89.1 [0.99]
87.9 [0.99]
SUC

Figure 3.

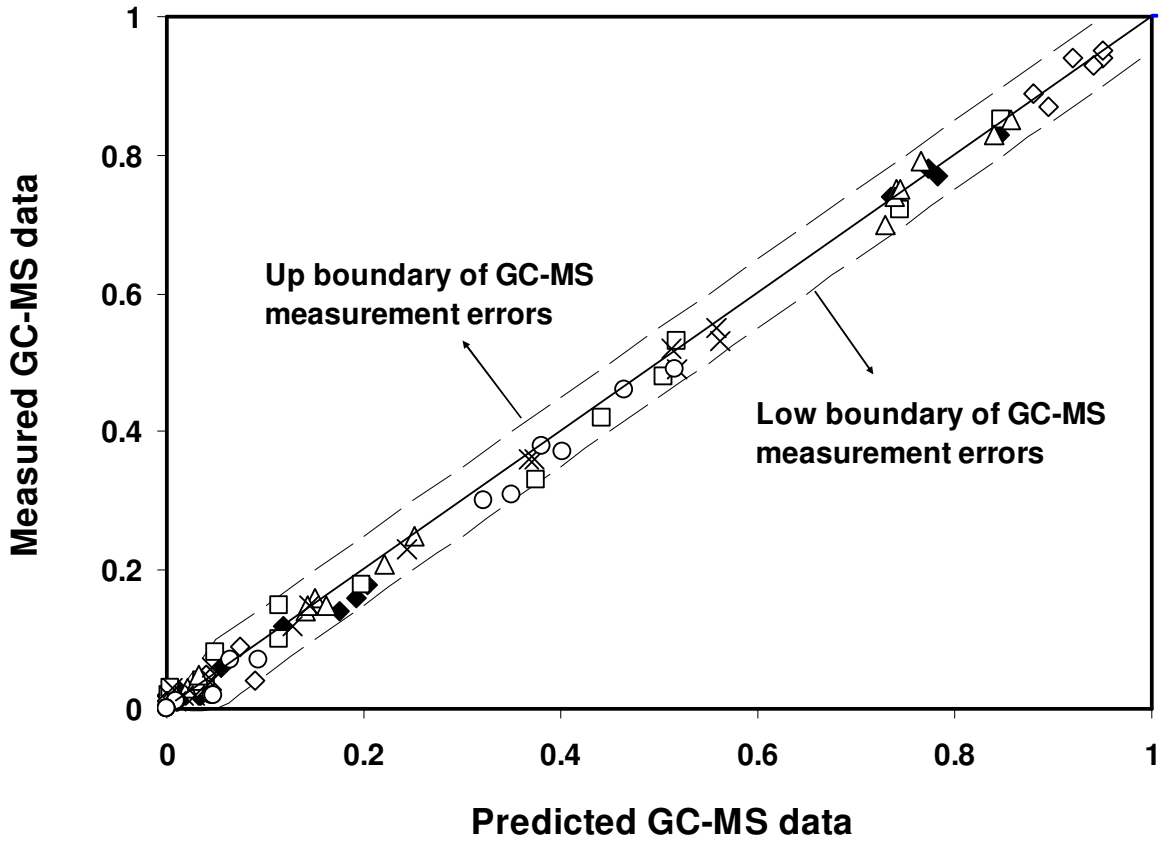
Measured GC-MS data
Predicted GC-MS data
Up boundary of GC-MS measurement errors
Low boundary of GC-MS measurement errors
0
0.2
0.4
0.6
0.8
1

Table 1. Measured and model predicted (in parenthesis) fragment mass distributions for ^{13}C-labeled metabolites from *Geobacter metallireducens* GS-15 hydrolysates[1].

Amino acids (Precursors)	Fragment	**1-^{13}C acetate culture**			
		M_0	M_1	M_2	M_3
Glycine (PEP)[2]	$(M57)^+$	0.15±0.02	0.85±0.03		
	$(M85)^+$	0.26±0.02	0.74±0.03		
Serine (PEP)	$(M57)^+$	0.14±0.02	0.83±0.03	0.03±0	
	$(M159)^+$	0.25±0.02	0.75±0.03	0.0±0	
Alanine (pyruvate)	$(M57)^+$	0.05±0.02	0.94±0.02	0.01±0	
	$(M159)^+$	0.05±0.02	0.95±0.01	0±0	
Leucine (pyruvate & acetyl CoA)	$(M159)^+$	0.01±0	0.09±0.02	0.87±0.02	0.02±0
Glutamate (OXO)	$(M57)^+$	0.02±0	0.77±0.03	0.14±0.02	0.03±0.01
	$(M159)^+$	0.02±0.01	0.83±0.02	0.12±0.02	0.02±0.01
Asparate (OAA)	$(M57)^+$	0.04±0.02	0.85±0.03	0.10±0.02	0.01±0
	$(M159)^+$	0.42±0.03	0.53±0.03	0.03±0.01	0.02±0.01
Histidine (C5P)	$(M57)^+$	0.04±0.01	0.36±0.02	0.55±0.02	0.02±0
	$(M159)^+$	0.06±0.02	0.36±0.02	0.53±0.02	0.02±0
Phenylalanine (PEP+E4P)	$(M57)^+$	0.01±0	0.07±0.01	0.29±0.04	0.49±0.05
	$(M159)^+$	0.01±0	0.07±0.01	0.31±0.04	0.46±0.05
Predicted CO_2		0.01			
Predicted C1pool		0.02			

Table 1 (Continued)

Amino acids (Precursors)	Fragment	2-^{13}C acetate culture			
		M_0	M_1	M_2	M_3
Glycine (PEP)[2]	$(M57)^+$	0.75±0.03	0.15±0.02	0.10±0.02	
	$(M85)^+$	0.79±0.03	0.21±0.02		
Serine (PEP)	$(M57)^+$	0.04±0.01	0.70±0.03	0.16±0.02	
	$(M159)^+$	0.05±0.02	0.79±0.03	0.16±0.02	
Alanine (pyruvate)	$(M57)^+$	0.03±0.01	0.93±0.01	0.02±0.01	
	$(M159)^+$	0.03±0	0.93±0.01	0.04±0.01	
Leucine (pyruvate & acetyl CoA)	$(M159)^+$	0.01±0	0.01±0	0.04±0.01	0.89±0.02
Glutamate (OXO)	$(M57)^+$	0.02±0	0.01±0	0.16±0.01	0.74±0.02
	$(M159)^+$	0.02±0	0.02±0	0.18±0.02	0.78±0.03
Asparate (OAA)	$(M57)^+$	0.02±0.01	0.08±0.01	0.18±0.02	0.72±0.03
	$(M159)^+$	0.03±0.02	0.15±0.02	0.48±0.02	0.33±0.02
Histidine (C5P)	$(M57)^+$	0.02±0	0.01±0	0.15±0.02	0.52±0.03
	$(M159)^+$	0.03±0.01	0.12±0.01	0.49±0.02	0.23±0.02
Phenylalanine (PEP+E4P)	$(M57)^+$	0.01±0	0±0	0.02±0	0.38±0.03
	$(M159)^+$	0.01±0	0±0	0.02±0	0.36±0.02
Predicted CO_2		0.03			
Predicted C1pool		0.82			

1. ^{13}C-Labeled biomass was sampled in the middle log phase. The standard deviations for GC-MS measurement were based on the triplicate experiments (n=3).

2. Glycine fragmentation $(M159)^+$ was not observed. $(M85)^+$ (Loss of carboxyl group) was used instead.